Robust Trust-Region Space-Mapping Algorithms for Microwave Design Optimization

Slawomir Koziel, *Senior Member, IEEE*, John W. Bandler, *Life Fellow, IEEE*, and Qingsha S. Cheng, *Senior Member, IEEE*

***Abstract*—Convergence is a well-known issue for standard space-mapping optimization algorithms. It is heavily dependent on the choice of coarse model, as well as the space-mapping transformations employed in the optimization process. One possible convergence safeguard is the trust region approach where a surrogate model is optimized in a restricted neighborhood of the current iteration point. In this paper, we demonstrate that although formal conditions for applying trust regions are not strictly satisfied for space-mapping surrogate models, the approach improves the overall performance of the space-mapping optimization process. Further improvement can be realized when approximate fine model Jacobian information is exploited in the construction of the space-mapping surrogate. A comprehensive numerical comparison between standard and trust-region-enhanced space mapping is provided using several examples of microwave design problems.**

***Index Terms*—Computer-aided design (CAD), electromagnetic (EM) optimization, microwave design, space mapping, trust-region methods.**

I. Introduction

SPACE-MAPPING technology is exploited both in microwave engineering and other areas [1]–[16] to deal with computationally expensive objective functions.

The main idea behind space-mapping optimization is to shift the optimization burden from an expensive "fine" (or high-fidelity) model to a cheap "coarse" (or low-fidelity) model by iteratively optimizing and updating a surrogate model, which is built using the coarse model and available fine model data. If the coarse model is a sufficiently accurate representation of the fine model, space-mapping optimization may yield a satisfactory solution after only a few fine model evaluations. This enjoys a substantial advantage over other techniques in terms of computational cost, such as direct optimization of the fine model using gradient-based methods. The idea of surrogate-based optimization is also exploited by other researchers [17]–[20], although many of them construct a surrogate model by direct approximation of the fine model data with no underlying physically based coarse model.

Probably the most serious issue for standard space mapping is convergence, depending on the similarity between the fine model and the space-mapping surrogate [3], [21]. Also, because the zero- and first-order consistency conditions [17] between the fine and surrogate models are not necessarily satisfied (i.e., the surrogate model may not match the fine model with respect to value and first-order derivative at any given iteration points), and subsequent iterations are accepted regardless of objective function improvement, there is no guarantee that the specification error will be reduced from iteration to iteration. In fact, after a few successful iterations, the space-mapping algorithm may produce a design that is worse than ones found so far [22].

Given an optimization problem, the convergence properties and overall performance of the space-mapping algorithm can be improved to some extent by a proper choice of the coarse model and the space-mapping surrogate [21], [23]. On the other hand, given the models and the mapping type, good algorithm performance (measured by convergence and final design quality) is not guaranteed and has to be verified experimentally by executing the optimization process.

Trust-region methodology [24] can be used to amend the convergence properties of space-mapping algorithms [23], [25]. Formally, using trust-region methods with space-mapping algorithms is not well justified because first-order consistency [17] between the fine model and space-mapping surrogate does not usually hold, and, therefore, trust-region methods for space mapping become heuristic rather than rigorous. More specifically, first-order consistency guarantees fine model objective function improvement provided that the trust-region radius is small enough [26]. Using trust-region methods in the space-mapping algorithm is justified by the fact that a physics-based surrogate model reflects the general features of the fine model so that their local behavior is similar. Nevertheless, the objective function improvement is not guaranteed regardless of how small the trust region is. First-order consistency can be enforced in the space-mapping surrogate by explicit use of sensitivity information [3]; however, this increases the overall cost of the space-mapping optimization process.

In this paper, we expand a systematic treatment of the trust-region-enhanced space-mapping algorithms originated in [22],

Manuscript received February 18, 2010; revised May 10, 2010; accepted May 21, 2010. Date of publication July 01, 2010; date of current version August 13, 2010. This work was supported in part by the Reykjavik University Development Fund under Grant T09009 and by the Natural Sciences and Engineering Research Council of Canada (NSERC) under Grant RGPIN7239-06 and Grant STPGP 381153-09.

S. Koziel is with the Engineering Optimization and Modeling Center, School of Science and Engineering, Reykjavik University, 101 Reykjavik, Iceland (e-mail: koziel@ru.is).

J. W. Bandler is with the Simulation Optimization Systems Research Laboratory, Department of Electrical and Computer Engineering, McMaster University, Hamilton, ON, Canada L8S 4K1, and also with Bandler Corporation, Dundas, ON, Canada L9H 5E7 (e-mail: bandler@mcmaster.ca).

Q. S. Cheng is with the Simulation Optimization Systems Research Laboratory, Department of Electrical and Computer Engineering, McMaster University, Hamilton, ON, Canada L8S 4K1 (e-mail: chengq@mcmaster.ca).

Color versions of one or more of the figures in this paper are available online at http://ieeexplore.ieee.org.

Digital Object Identifier 10.1109/TMTT.2010.2052666

where we gave a heuristic explanation of why the trust region actually works with space-mapping algorithms, as well as proposed a modification of the trust-region-enhanced space-mapping algorithm, which uses an approximate fine model Jacobian to enhance the surrogate model. Here, alternative ways of creating surrogate models exploiting the fine model Jacobian estimation are described. Also, additional in-depth analysis of the trust-region-based space-mapping algorithms is presented. In particular, an analytical argument is given to support the expected performance improvement for the algorithm using the approximated fine model Jacobian.

A comprehensive numerical comparison between the standard and the three variants of the trust-region-enhanced space-mapping algorithm is provided based on several examples of microwave design optimization problems. It is demonstrated that the trust-region-enhancement indeed improves the robustness of the space-mapping optimization process with respect to all performance measures: the quality of the optimized design, the convergence properties, and the computational cost of the optimization process.

II. Space Mapping With Trust-Region Convergence Safeguards

A. Standard Space-Mapping Algorithm

Let $\boldsymbol{R}_f : X_f \rightarrow R^m$, $X_f \subseteq R^n$ denote the response vector of a fine model of the device of interest. Our goal is to solve

$$\boldsymbol{x}_f^* = \arg\min_{\boldsymbol{x}\in X_f} U(\boldsymbol{R}_f(\boldsymbol{x})) \tag{1}$$

where U: $R^m \rightarrow R$ is a given objective function, e.g., minimax [1].

Direct optimization of the fine model is replaced by an iterative procedure generating a sequence of designs $\boldsymbol{x}^{(i)} \in X_f$, $i = 0, 1, 2, \ldots$, and a family of surrogate models $\boldsymbol{R}_s^{(i)} : X_s^{(i)} \rightarrow R^m$, $X_s^{(i)} \subseteq R^n$, $i = 0, 1, \ldots$, so that

$$\boldsymbol{x}^{(i+1)} = \arg\min_{\boldsymbol{x}} U\left(\boldsymbol{R}_s^{(i)}(\boldsymbol{x})\right). \tag{2}$$

Let $\boldsymbol{R}_c : X_c \rightarrow R^m$, $X_c \subseteq R^n$ denote the response vectors of the coarse model that describes the same object as the fine model: less accurate, but much faster to evaluate. Surrogate models $\boldsymbol{R}_s^{(i)}$ in (2) are constructed as follows:

$$\boldsymbol{R}_s^{(i)}(\boldsymbol{x}) = \bar{\boldsymbol{R}}_s(\boldsymbol{x}, \boldsymbol{p}^{(i)}) \tag{3}$$

where $\bar{\boldsymbol{R}}_s : X_s \rightarrow R^m$ is a generic space-mapping surrogate model, which is $\boldsymbol{R}_c$ composed with some suitable space-mapping transformations, and $X_s \subseteq X_c \times X_p$ with X_p being the parameter space of these transformations. A vector of space-mapping parameters, $\boldsymbol{p}^{(i)}$, is obtained using the parameter extraction procedure

$$\boldsymbol{p}^{(i)} = \arg\min_{\boldsymbol{p}} \sum_{k=0}^{i} ||\boldsymbol{R}_f(\boldsymbol{x}^{(k)}) - \bar{\boldsymbol{R}}_s(\boldsymbol{x}^{(k)}, \boldsymbol{p})||. \tag{4}$$

An example of the generic surrogate model is an input space mapping of the form $\boldsymbol{x} \rightarrow \boldsymbol{B}\boldsymbol{x} + \boldsymbol{c}$, where $\bar{\boldsymbol{R}}_s(\boldsymbol{x}, \boldsymbol{p}) = \bar{\boldsymbol{R}}_s(\boldsymbol{x}, \boldsymbol{B}, \boldsymbol{c}) = \boldsymbol{R}_c(\boldsymbol{B} \cdot \boldsymbol{x} + \boldsymbol{c})$. A variety of other space-mapping surrogates can be found in [1]–[4], [27].

B. Robustness Issues

As the algorithm (2)–(4) accepts a new design $\boldsymbol{x}^{(i+1)}$ regardless of the $\boldsymbol{R}_f$ specification error improvement, convergence of the space-mapping algorithm is not guaranteed [1]. Moreover, as a perfect match between $\boldsymbol{R}_s^{(i)}$ and $\boldsymbol{R}_f$ at $\boldsymbol{x}^{(i)}$ is not ensured (with respect to value and/or first-order derivatives), there is no guarantee for the space-mapping algorithm to locate the (local) fine model optimal solution [21].

Existing theoretical results for algorithm (2)–(4) or some of its sub-classes provide convergence conditions, which are, however, difficult to verify beforehand [3], [21]. Moreover, conditions for convergence are typically different from conditions for convergence to the fine model optimal solution (i.e., its first-order stationary point) [21]. This is because fine model sensitivity information is not utilized by current space-mapping algorithms.

Excellent results reported in the literature [1]–[13], obtained with space-mapping algorithms, are largely dependent on carefully chosen coarse models and properly selected space-mapping type. No safeguard is offered in the standard space mapping for a not-so-well-selected coarse model or/and a mapping type.

C. Trust-Region Enhanced Space-Mapping Algorithm

A trust-region approach [24] can be used to improve the convergence properties of the space-mapping algorithm. In particular, the surrogate optimization process (2) can be constrained to a neighborhood of $\boldsymbol{x}^{(i)}$, defined as $\|\boldsymbol{x} - \boldsymbol{x}^{(i)}\| \leq \delta^{(i)}$, as follows

$$\boldsymbol{x}^{(i+1)} = \arg\min_{\boldsymbol{x}, ||\boldsymbol{x}-\boldsymbol{x}^{(i)}|| < \delta^{(i)}} U\left(\boldsymbol{R}_s^{(i)}(\boldsymbol{x})\right) \tag{5}$$

where $\delta^{(i)}$ is a trust-region radius at iteration i. The trust-region radius is reduced if the improvement of the fine model objective function is not sufficient, i.e., if $(U(\boldsymbol{R}_f(\boldsymbol{x}^{(i+1)})) - U(\boldsymbol{R}_f(\boldsymbol{x}^{(i)})))/(U(\boldsymbol{R}_s^{(i)}(\boldsymbol{x}^{(i+1)})) - U(\boldsymbol{R}_s^{(i)}(\boldsymbol{x}^{(i)})))$ is too small, or if $U(\boldsymbol{R}_f(\boldsymbol{x}^{(i+1)})) \geq U(\boldsymbol{R}_f(\boldsymbol{x}^{(i)}))$, in which case the new design is rejected. Typically, the standard trust-region radius updating rules [24] are used.

If, for all $i = 0, 1, 2, \ldots$, the surrogate model satisfies the zeroth- and first-order consistency conditions of the form

$$\boldsymbol{R}_s^{(i)}(\boldsymbol{x}^{(i)}) = \boldsymbol{R}_f(\boldsymbol{x}^{(i)}) \tag{6}$$

$$\boldsymbol{J}_{\boldsymbol{R}_s^{(i)}}(\boldsymbol{x}^{(i)}) = \boldsymbol{J}_{\boldsymbol{R}_f}(\boldsymbol{x}^{(i)}) \tag{7}$$

where $\boldsymbol{J}$ denotes the Jacobian of the respective model, then, under mild assumptions concerning smoothness of the models, algorithm (5) is convergent to the local fine model optimum [26]. The fundamental reason is that (6) and (7) ensure that $U(\boldsymbol{R}_f(\boldsymbol{x}^{(i+1)})) < U(\boldsymbol{R}_f(\boldsymbol{x}^{(i)}))$ if the trust-region radius is sufficiently small.

Unfortunately, (6) and (7) are not necessarily satisfied by the space-mapping surrogate model. In particular, the space-mapping optimization process may get stuck at some point as the reduction of the trust-region radius $\delta^{(i)}$ does not bring any improvement to the fine model objective function, which results in termination of the algorithm. In other words, the trust-region method applied to the space-mapping algorithm, as in (5), is a

heuristic procedure that may improve robustness of the algorithm, but still does not ensure sufficient performance.

On the other hand, an important prerequisite of space-mapping algorithms is that $\boldsymbol{R}_c$ is physics based so that the surrogate model reflects the general features of $\boldsymbol{R}_f$; in particular, the local behavior of both models is similar. This, in combination with the multipoint parameter extraction (4), ensures that (6) and (7) may be satisfied approximately. Moreover, condition (6) can be easily enforced by means of the output space mapping [3] using the surrogate

$$\boldsymbol{R}_s^{(i)}(\boldsymbol{x}) = \bar{\boldsymbol{R}}_s(\boldsymbol{x}, \boldsymbol{p}^{(i)}) + \boldsymbol{d}^{(i)} \tag{8}$$

with $\boldsymbol{p}^{(i)}$ obtained by (4) and

$$\boldsymbol{d}^{(i)} = \boldsymbol{R}_f(\boldsymbol{x}^{(i)}) - \bar{\boldsymbol{R}}_s(\boldsymbol{x}^{(i)}, \boldsymbol{p}^{(i)}). \tag{9}$$

Numerical results presented in Section IV demonstrate that the trust-region-enhanced (output) space-mapping algorithm (8) and (9) indeed exhibits improvement over the standard algorithm.

III. Robust Trust-Region Space-Mapping Algorithms

Relations (6) and (7) can be enforced if the space-mapping surrogate explicitly uses fine model sensitivity information, e.g., as in the following model:

$$\boldsymbol{R}_s^{(i)}(\boldsymbol{x}) = \bar{\boldsymbol{R}}_s(\boldsymbol{x}, \boldsymbol{p}^{(i)}) + \boldsymbol{d}^{(i)} + \boldsymbol{E}^{(i)} \cdot (\boldsymbol{x} - \boldsymbol{x}^{(i)}) \tag{10}$$

where $\bar{\boldsymbol{R}}(\boldsymbol{x}, \boldsymbol{p}^{(i)})$ is any space-mapping surrogate with parameters $\boldsymbol{p}^{(i)}$ obtained with (4) and

$$\boldsymbol{d}^{(i)} = \boldsymbol{R}_f(\boldsymbol{x}^{(i)}) - \bar{\boldsymbol{R}}_s(\boldsymbol{x}^{(i)}, \boldsymbol{p}^{(i)}) \tag{11}$$

$$\boldsymbol{E}^{(i)} = \boldsymbol{J}_{\boldsymbol{R}_f}(\boldsymbol{x}^{(i)}) - \boldsymbol{J}_{\bar{\boldsymbol{R}}_s(\cdot, \boldsymbol{p}^{(i)})}(\boldsymbol{x}^{(i)}). \tag{12}$$

Convergence of algorithm (5) with surrogate model (10)–(12) is guaranteed under standard assumptions concerning the smoothness of the fine and coarse models [26]. Note, however, that the computational cost of space-mapping optimization may substantially increase in this case because of the necessity of calculating the fine model Jacobian at all iterations. Jacobian estimation using finite differences exploits extra n fine model evaluations per estimation, unless some other techniques are used, such as adjoint sensitivity [28], which, however, is not yet generally available in commercial electromagnetic (EM) simulators.

In this section, we propose some modifications of the standard trust-region space-mapping algorithm that aim at ensuring robustness of the algorithm without compromising the computational cost of the algorithm, i.e., avoiding explicit calculation of the fine model Jacobian. All the proposed algorithms are based on modifications of the surrogate model (10)–(12) so that the exact fine model sensitivity data is replaced by a suitable approximation.

Before we turn to specific models, let us discuss a naive approach, according to which the surrogate model Jacobian is calculated using finite differences, whereas the fine model Jacobian in (12) is replaced by a Broyden-based estimation (the iterative formula for estimating the fine model Jacobian) [2], [29], i.e., we have

$$\boldsymbol{E}^{(i)} = \boldsymbol{J}^{(i)}_{\boldsymbol{B}.\boldsymbol{R}_f} - \boldsymbol{J}_{\bar{\boldsymbol{R}}_s(\cdot, \boldsymbol{p}^{(i)})}(\boldsymbol{x}^{(i)}) \tag{13}$$

where the Broyden-based fine model Jacobian estimation

$$\boldsymbol{J}^{(i)}_{\boldsymbol{B}.\boldsymbol{R}_f} = \boldsymbol{J}^{(i-1)}_{\boldsymbol{B}.\boldsymbol{R}_f} + \frac{\left(\boldsymbol{f}^{(i)} - \boldsymbol{J}^{(i-1)}_{\boldsymbol{B}.\boldsymbol{R}_f} \cdot \boldsymbol{h}^{(i)}\right) \cdot \boldsymbol{h}^{(i)T}}{\boldsymbol{h}^{(i)T}\boldsymbol{h}^{(i)}}, \quad i = 1, 2, \ldots \tag{14}$$

with $\boldsymbol{f}^{(i)} = \boldsymbol{R}_f(\boldsymbol{x}^{(i)}) - \boldsymbol{R}_f(\boldsymbol{x}^{(i-1)})$, $\boldsymbol{h}^{(i)} = \boldsymbol{x}^{(i)} - \boldsymbol{x}^{(i-1)}$, and $\boldsymbol{J}^{(0)}_{\boldsymbol{B}.\boldsymbol{R}_f} = 0_{m\times n}$ ($0_{m\times n}$ is an $m \times n$ zero matrix, where m is the dimension of the model response).

Unfortunately, model (10), (11), and (13) will not work well in practice. The reason is that $\boldsymbol{J}^{(i)}_{\boldsymbol{B}.\boldsymbol{R}_f}$ contains information about the fine model Jacobian at $\boldsymbol{x}^{(i)}$ only for directions from $X_h^{(i)} = \mathrm{span}(\boldsymbol{h}^{(1)}, \boldsymbol{h}^{(2)}, \ldots, \boldsymbol{h}^{(i)})$, i.e., the subspace of R^n spanned by vectors $\boldsymbol{h}^{(1)}$ to $\boldsymbol{h}^{(i)}$. As (14) is a rank-one formula, we need at least n iterations of the space-mapping algorithm in order to get an estimate of the fine model Jacobian that would be valid for all directions. Before that, the term $\boldsymbol{E}^{(i)}$ may actually mislead the algorithm because $\boldsymbol{J}^{(i)}_{\boldsymbol{B}.\boldsymbol{R}_f} \cdot \boldsymbol{h}$ is a zero vector for all directions $\boldsymbol{h}$ not belonging to $X_h^{(i)}$ so that the directional derivative of (10) for such directions may substantially differ from the actual derivative of the fine model.[1] Moreover, even if i is sufficiently large, so that $X_h^{(i)}$ spans the entire R^n space, estimate (14) may not be sufficiently accurate as many of the points used in the Broyden update may be located too far from $\boldsymbol{x}^{(i)}$.

A. Surrogate Model With Restricted Broyden Update

The trust-region space-mapping algorithm with Broyden update can be improved if the $\boldsymbol{E}^{(i)}$ term (13) is restricted to the subspace $X_h^{(i)}$ so that $\boldsymbol{E}^{(i)} \cdot (\boldsymbol{x} - \boldsymbol{x}^{(i)}) = 0$ for all $\boldsymbol{x} - \boldsymbol{x}^{(i)}$ from $X_h^{(i)\perp}$, the orthogonal complement of $X_h^{(i)}$, defined as $X_h^{(i)\perp} = \{\boldsymbol{x} \in R^n : \boldsymbol{x} \perp \boldsymbol{y} \text{ for all } \boldsymbol{y} \in X_h^{(i)}\}$. In this case, the derivative of $\boldsymbol{R}_s^{(i)}$ at $\boldsymbol{x}^{(i)}$ will coincide with the derivative of $\bar{\boldsymbol{R}}_s(\boldsymbol{x}^{(i)}, \boldsymbol{p}^{(i)})$ for all directions from $X_h^{(i)\perp}$, but it will use the Jacobian estimation of the fine model for all directions from $X_h^{(i)}$. An appropriate formula is as follows:

$$\boldsymbol{E}^{(i)} = \left(\boldsymbol{J}^{(i)}_{\boldsymbol{B}.\boldsymbol{R}_f} - \boldsymbol{J}_{\bar{\boldsymbol{R}}_s(\cdot, \boldsymbol{p}^{(i)})}(\boldsymbol{x}^{(i)})\right) \boldsymbol{P}_{X_h^{(i)}} \tag{15}$$

where $\boldsymbol{J}^{(i)}_{\boldsymbol{B}.\boldsymbol{R}_f}$ is given by (14), whereas $\boldsymbol{P}_{X_h^{(i)}}$ is an orthogonal projection onto $X_h^{(i)}$ given by

$$\boldsymbol{P}_{X_h^{(i)}} = \sum_{k=1}^{i} \boldsymbol{v}^{(k)} \boldsymbol{v}^{(k)T} \tag{16}$$

with $\boldsymbol{v}^{(k)}$, $k = 1, 2, \ldots$, being the orthonormal basis of $X_h^{(i)}$ that can be obtained from $\boldsymbol{h}^{(k)}$, $k = 1, 2, \ldots$, using the Gram–Schmidt procedure.

[1] In fact, the directional derivative of (10) equals zero at $\boldsymbol{x}^{(i)}$ for all directions not belonging to $X_h^{(i)}$ and it is close to zero in the neighborhood of $\boldsymbol{x}^{(i)}$.

Equation (15) basically says that we trust the fine model Jacobian in directions where fine model data is available, however, the fine model Jacobian should match the surrogate Jacobian in directions of "no data." It can be further improved by using only points that are sufficiently close to $\boldsymbol{x}^{(i)}$ so that instead of considering $X_h^{(i)} = \text{span}(\boldsymbol{h}^{(1)}, \boldsymbol{h}^{(2)}, \ldots, \boldsymbol{h}^{(i)})$, we can consider the subspace spanned only by those of $\boldsymbol{h}^{(k)}$ that satisfy $\|\boldsymbol{h}^{(k)}\| \leq r^{(i)}$, where $r^{(i)}$ is a user-defined threshold; $r^{(i)}$ can be either fixed, i.e., $r^{(i)} = C_1$, or it can be related to the distance between the latest iteration designs, i.e., $r^{(i)} = C_2 \cdot \|\boldsymbol{x}^{(i)} - \boldsymbol{x}^{(i-1)}\|$, where C_1 and C_2 are user-defined positive numbers.

B. Surrogate Model With Broyden-Based Jacobian Estimation of the Fine and Surrogate Model [22]

Restriction of the $\boldsymbol{E}^{(i)}$ term (13) to the subspace $X_h^{(i)}$ can also be obtained if the Jacobians of the fine model and the space-mapping surrogate $\bar{\boldsymbol{R}}_s(\boldsymbol{x}, \boldsymbol{p}^{(i)})$ are estimated jointly using the Broyden update, i.e., with the following formula [22]:

$$\boldsymbol{E}^{(i)} = \boldsymbol{J}^{(i)}_{\boldsymbol{B}.\boldsymbol{R}_f - \bar{\boldsymbol{R}}_s} \tag{17}$$

where

$$\boldsymbol{J}^{(i)}_{\boldsymbol{B}.\boldsymbol{R}_f - \bar{\boldsymbol{R}}_s} = \boldsymbol{J}^{(i-1)}_{\boldsymbol{B}.\boldsymbol{R}_f - \bar{\boldsymbol{R}}_s} + \frac{\left(\bar{\boldsymbol{f}}^{(i)} - \boldsymbol{J}^{(i-1)}_{\boldsymbol{B}.\boldsymbol{R}_f - \bar{\boldsymbol{R}}_s} \cdot \boldsymbol{h}^{(i)}\right) \cdot \boldsymbol{h}^{(i)T}}{\boldsymbol{h}^{(i)T}\boldsymbol{h}^{(i)}} \tag{18}$$

with $\bar{\boldsymbol{f}}^{(i)} = (\boldsymbol{R}_f(\boldsymbol{x}^{(i)}) - \bar{\boldsymbol{R}}_s(\boldsymbol{x}^{(i)}, \boldsymbol{p}^{(i)})) - (\boldsymbol{R}_f(\boldsymbol{x}^{(i-1)}) - \bar{\boldsymbol{R}}_s(\boldsymbol{x}^{(i-1)}, \boldsymbol{p}^{(i)}))$, $\boldsymbol{h}^{(i)} = \boldsymbol{x}^{(i)} - \boldsymbol{x}^{(i-1)}$, and $\boldsymbol{J}^{(0)}_{\boldsymbol{B}.\boldsymbol{R}_f - \bar{\boldsymbol{R}}_s} = 0_{m \times n}$. In this case, we do not need to project $\boldsymbol{E}^{(i)}$ onto $X_h^{(i)}$ as the condition $\boldsymbol{E}^{(i)} \cdot (\boldsymbol{x} - \boldsymbol{x}^{(i)}) = 0$ for all $\boldsymbol{x} - \boldsymbol{x}^{(i)}$ from $X_h^{(i)\perp}$ is automatically fulfilled.

As before, it is recommended to consider local updates using points satisfying $\|\boldsymbol{x}^{(k)} - \boldsymbol{x}^{(i)}\| \leq r^{(i)}$, where $r^{(i)}$ is a user-defined threshold (either fixed or relative to $\|\boldsymbol{x}^{(i)} - \boldsymbol{x}^{(i-1)}\|$).

It should be noted that (15)–(18) are two alternative methods of determining the term $\boldsymbol{E}^{(i)}$ in (10); however, it is difficult to say beforehand which is better in terms of algorithm performance. The numerical experiments of Section IV indicate that both methods are comparable.

C. Robustness of Trust-Region Space-Mapping Algorithms

Note that in contrast to our standard trust-region space-mapping algorithm (5), the modifications proposed in this section ensure improvement of the fine model objective function for sufficiently small trust-region radius, which is a fundamental property behind the trust-region methodology. In particular, for the algorithms using the $\boldsymbol{E}$ term defined in Sections III-A and III-B. we have $U(\boldsymbol{R}_f(\boldsymbol{x}^{(i+1)})) < U(\boldsymbol{R}_f(\boldsymbol{x}^{(i)}))$ ($\boldsymbol{x}^{(i+1)}$ and $\boldsymbol{x}^{(i)}$ are two consecutive iteration points) provided that the trust-region radius $\delta^{(i)}$ is sufficiently small. A sketch of this property is provided in the Appendix.

IV. Verification Examples

We provide a comprehensive numerical verification of the trust-region-enhanced space-mapping algorithms. In particular, we compare the performance of the standard space-mapping (SM_{STD}) algorithm (2)–(4), the trust-region-enhanced space-mapping (SM_{TR}) algorithm (5) with the output space-mapping model (8), (9), and the trust-region-enhanced algorithms using models (10), (11), (15) ($\text{SM}_{\text{TR-B1}}$) and (10), (11), (17) ($\text{SM}_{\text{TR-B2}}$). In all cases, the algorithm was terminated if one of the following conditions was satisfied: $\|\boldsymbol{x}^{(i+1)} - \boldsymbol{x}^{(i)}\| < 10^{-2}$, $\delta^{(i+1)} < 10^{-3}$, or $U(\boldsymbol{R}_f(\boldsymbol{x}^{(i)})) - U(\boldsymbol{R}_f(\boldsymbol{x}^{(i+1)})) < 10^{-2}$ (SM_{TR}, $\text{SM}_{\text{TR-B1}}$, and $\text{SM}_{\text{TR-B2}}$ only).

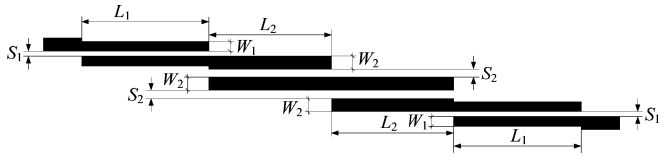

Fig. 1. Third-order Chebyshev bandpass filter: geometry [30].

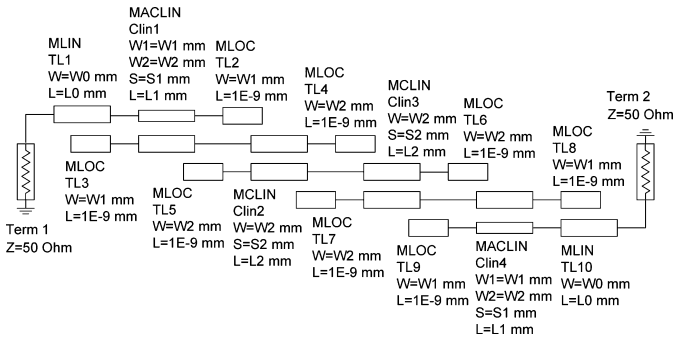

Fig. 2. Third-order Chebyshev bandpass filter: coarse model (Agilent ADS).

A. Third-Order Chebyshev Bandpass Filter [30]

Consider the third-order Chebyshev bandpass filter [30] shown in Fig. 1. The design variables are $\boldsymbol{x} = [L_1 L_2 S_1 S_2]^T$ mm. Other parameters are $W_1 = W_2 = 0.4$ mm. The fine model $\boldsymbol{R}_f$ is simulated in Sonnet *em* [31]. The coarse model (Fig. 2) is implemented in Agilent Advanced Design System (ADS) [32]. The design specifications are $|S_{21}| \geq -3$ dB for 1.8 GHz $\leq \omega \leq$ 2.2 GHz, and $|S_{21}| \leq -20$ dB for 1.0 GHz $\leq \omega \leq$ 1.6 GHz and 2.4 GHz $\leq \omega \leq$ 3.0 GHz. The initial design is the coarse model optimal solution $\boldsymbol{x}^{(0)} = [14.7\ 15.3\ 0.62\ 0.50]^T$ mm (specification error + 7.2 dB).

Table I shows the optimization results. Two types of space-mapping surrogate models were tested: input space-mapping model $\bar{\boldsymbol{R}}_s(\boldsymbol{x}) = \boldsymbol{R}_c(\boldsymbol{x} + \boldsymbol{c})$ [2] and the combination of input and frequency space-mapping model $\bar{\boldsymbol{R}}_s(\boldsymbol{x}) = \boldsymbol{R}_{c.F}(\boldsymbol{x} + \boldsymbol{c})$ in which $\boldsymbol{R}_{c.F}$ is the coarse model evaluated at frequencies different from the original sweep according to the linear mapping $\omega \longrightarrow f_1 + f_2\omega$ [parameters f_1 and f_2 are obtained using the usual parameter-extraction process (4)] [3].

For this example, the standard space-mapping algorithm converges for both surrogate model types, however, especially for the input space-mapping model $\boldsymbol{R}_c(\boldsymbol{x}+\boldsymbol{c})$, the final design is not as good as for trust-region-enhanced algorithms, particularly the ones using the Jacobian estimation. Fig. 3 shows the initial fine

TABLE I
THIRD-ORDER CHEBYSHEV FILTER: OPTIMIZATION RESULTS [22]

Surrogate Model	SM Algorithm	Specification Error		Number of Fine Model Evaluations
		Final	Best Found	
$\boldsymbol{R}_c(\boldsymbol{x}+\boldsymbol{c})$	SM_{STD}	–0.1	–0.1	8
	SM_{TR}	–0.1	–0.1	8
	SM_{TR-B1}	–1.0	–1.0	11
	SM_{TR-B2}	–1.0	–1.0	10
$\boldsymbol{R}_{c.F}(\boldsymbol{x}+\boldsymbol{c})$	SM_{STD}	–0.4	–0.7	8
	SM_{TR}	–0.7	–0.7	7
	SM_{TR-B1}	–0.7	–0.7	7
	SM_{TR-B2}	–0.7	–0.7	8

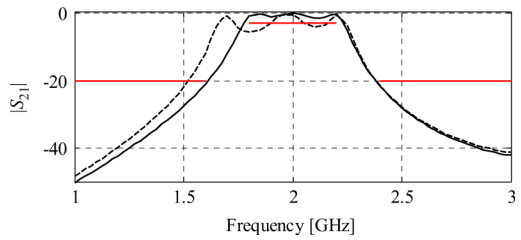

Fig. 3. Third-order Chebyshev filter: Initial (dashed line) and optimized (solid line) $|S_{21}|$ versus frequency; optimization using $\mathrm{SM_{TR-B2}}$ algorithm with the $\boldsymbol{R}_c(\boldsymbol{x}+\boldsymbol{c})$ model [22].

TABLE II
FOURTH-ORDER RING RESONATOR FILTER: OPTIMIZATION RESULTS

Surrogate Model	SM Algorithm	Specification Error		Number of Fine Model Evaluations
		Final	Best Found	
$\boldsymbol{R}_c(\boldsymbol{x}+\boldsymbol{c})$	SM_{STD}	–0.2	–0.3	21#
	SM_{TR}	–0.5	–0.5	18
	SM_{TR-B1}	–0.4	–0.4	21#
	SM_{TR-B2}	–0.4	–0.4	17
$\boldsymbol{R}_{c.f}(\boldsymbol{x})$	SM_{STD}	+0.2	–0.3	21#
	SM_{TR}	–0.1	–0.1	16
	SM_{TR-B1}	–0.4	–0.4	14
	SM_{TR-B2}	–0.4	–0.4	16

Convergence not obtained; algorithm terminated after 20 iterations.

model response and the optimized fine model response obtained using the $\mathrm{SM_{TR-B2}}$ algorithm with the $\boldsymbol{R}_c(\boldsymbol{x}+\boldsymbol{c})$ model.

B. Fourth-Order Ring Resonator Bandpass Filter [33]

As the next example, consider the fourth-order ring resonator bandpass filter [33] shown in Fig. 4. The design parameters are $\boldsymbol{x} = [L_1\ L_2\ L_3\ S_1\ S_2\ W_1\ W_2]^T$ mm. The fine model $\boldsymbol{R}_f$ is simulated in FEKO [34]. The coarse model (Fig. 5) is implemented in Agilent ADS [32]. The design specifications are $|S_{21}| \geq -1$ dB for 1.75 GHz $\leq \omega \leq$ 2.25 GHz, and $|S_{21}| \leq -20$ dB for 1.0 GHz $\leq \omega \leq$ 1.5 GHz and 2.5 GHz $\leq \omega \leq$ 3.0 GHz. The initial design is the coarse model optimal solution $\boldsymbol{x}^{(0)} = [24.74\ 19.51\ 24.10\ 0.293\ 0.173\ 1.232\ 0.802]^T$ mm (specification error + 9.0 dB).

Table II shows the optimization results. Here, we consider the following space-mapping surrogate models: the input space-mapping model $\bar{\boldsymbol{R}}_s(\boldsymbol{x}) = \boldsymbol{R}_c(\boldsymbol{x}+\boldsymbol{c})$[2] and the implicit space-mapping model $\bar{\boldsymbol{R}}_s(\boldsymbol{x}) = \boldsymbol{R}_{c.I}(\boldsymbol{x})$ in which $\boldsymbol{R}_{c.I}$ is the coarse model with the substrate height and dielectric constants used as preassigned parameters [27] to improve the matching between the surrogate and fine model.

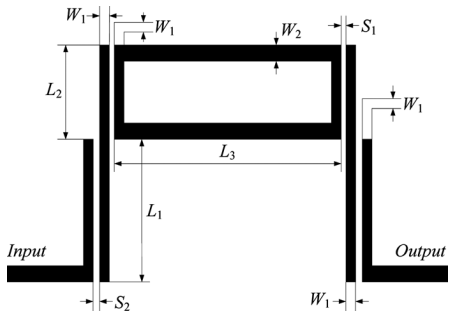

Fig. 4. Fourth-order ring resonator bandpass filter: geometry [33].

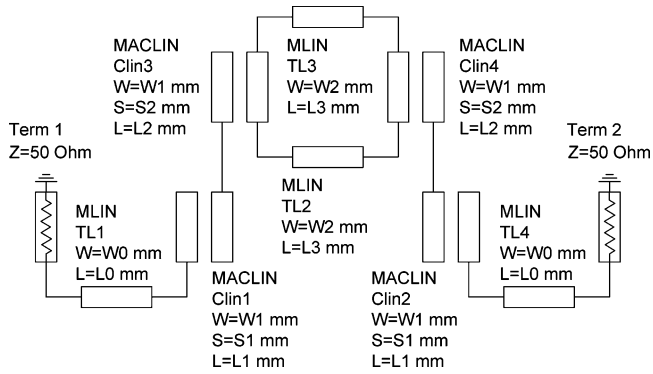

Fig. 5. Fourth-order ring resonator bandpass filter: coarse model (Agilent ADS).

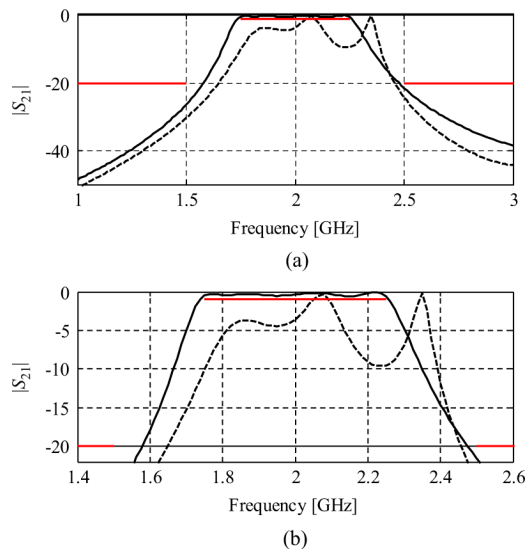

Fig. 6. Fourth-order ring resonator filter: initial (dashed line) and optimized (solid line) $|S_{21}|$ versus frequency; optimization using $\mathrm{SM_{TR-B2}}$ algorithm with the $\boldsymbol{R}_c(\boldsymbol{x}+\boldsymbol{c})$ model. (a) Full frequency range. (b) Magnification from 1.4 to 2.6 GHz and −22 to 0 dB.

Fig. 6 shows the initial fine model response and the optimized fine model response obtained using the $\mathrm{SM_{TR-B2}}$ algorithm with the $\boldsymbol{R}_c(\boldsymbol{x}+\boldsymbol{c})$ model. Fig. 7 shows the convergence plot for the standard algorithm and the $\mathrm{SM_{TR-B2}}$ algorithm both working with the implicit space-mapping surrogate $\boldsymbol{R}_{c.I}(\boldsymbol{x})$.

For this example, the standard space-mapping algorithm does not converge for either surrogate model type. Also, the final design is worse than the best one found in the course of optimiza-

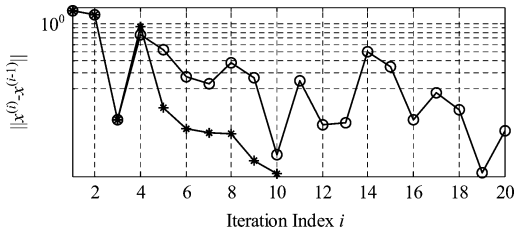

Fig. 7. Fourth-order ring resonator filter: convergence plots for $\mathrm{SM_{STD}}(o)$ and $\mathrm{SM_{TR-B2}}(*)$, both using surrogate model $\boldsymbol{R}_{c.I}(\boldsymbol{x})$, versus iteration index.

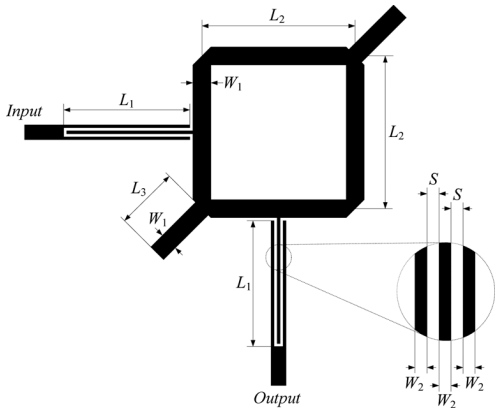

Fig. 8. Wideband ring resonator bandpass filter: geometry [35].

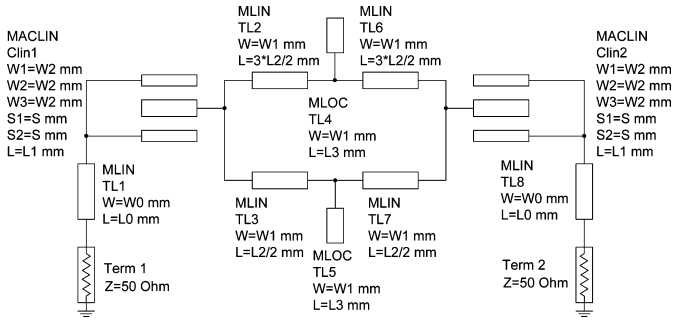

Fig. 9. Wideband ring resonator bandpass filter: coarse model (Agilent ADS).

TABLE III
WIDEBAND RING RESONATOR FILTER: OPTIMIZATION RESULTS

Surrogate Model	SM Algorithm	Specification Error		Number of Fine Model Evaluations
		Final	Best Found	
$\boldsymbol{R}_{c.F}(\boldsymbol{x}+\boldsymbol{c})$	$\mathrm{SM_{STD}}$	+6.7	+0.5	21#
	$\mathrm{SM_{TR}}$	–0.4	–0.4	9
	$\mathrm{SM_{TR-B1}}$	–0.4	–0.4	11
	$\mathrm{SM_{TR-B2}}$	–0.5	–0.5	13
$\boldsymbol{R}_{c.I}(\boldsymbol{x})$	$\mathrm{SM_{STD}}$	+1.3	–0.5	21#
	$\mathrm{SM_{TR}}$	–0.5	–0.5	9
	$\mathrm{SM_{TR-B1}}$	–0.5	–0.5	10
	$\mathrm{SM_{TR-B2}}$	–0.5	–0.5	11

Convergence not obtained; algorithm terminated after 20 iterations.

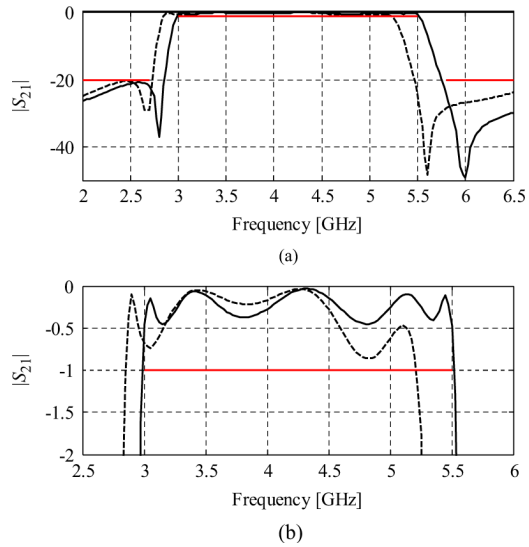

Fig. 10. Wideband ring resonator filter: initial (dashed line) and optimized (solid line) $|S_{21}|$ versus frequency; optimization using $\mathrm{SM_{TR-B2}}$ algorithm with the $\boldsymbol{R}_{c.I}(\boldsymbol{x})$ model. (a) Full frequency range. (b) Magnification from 2.5 to 6.0 GHz and -2 to 0 dB.

tion, which is because the standard algorithm does not ensure specification error improvement from iteration to iteration, as discussed in Section II. Trust-region-enhanced algorithms exhibit clear performance improvement.

C. Wideband Ring Resonator Bandpass Filter [35]

Our third example is the wideband ring resonator bandpass filter [35] shown in Fig. 8. The design parameters are $\boldsymbol{x} = [L_1\ L_2\ L_3\ W_1\ W_2\ S]^T$ mm. The fine model is simulated in FEKO [34]. The coarse model (Fig. 9) is implemented in Agilent ADS [32]. The design specifications are $|S_{21}| \geq -1$ dB for 3.0 GHz $\leq \omega \leq$ 5.5 GHz, and $|S_{21}| \leq -20$ dB for 2.0 GHz $\leq \omega \leq$ 2.7 GHz and 5.8 GHz $\leq \omega \leq$ 6.5 GHz. The initial design is the coarse model optimal solution $\boldsymbol{x}^{(0)} = [6.803\ \ 6.179\ \ 4.598\ \ 0.615\ \ 0.050\ \ 0.159]^T$ mm (specification error + 23.6 dB).

For this example, the following space-mapping surrogate models were utilized: the combination of the input and frequency space-mapping model $\bar{\boldsymbol{R}}_s(\boldsymbol{x}) = \boldsymbol{R}_{c.F}(\boldsymbol{x}+\boldsymbol{c})$ in which $\boldsymbol{R}_{c.F}$ is the frequency-mapped coarse model [3], and the implicit space-mapping model $\bar{\boldsymbol{R}}_s(\boldsymbol{x}) = \boldsymbol{R}_{c.I}(\boldsymbol{x})$ in which $\boldsymbol{R}_{c.I}$ is the coarse model with the substrate height and dielectric constants used as preassigned parameters [27].

Table III shows the optimization results. The standard space-mapping algorithm does not perform well. For the input/frequency space-mapping surrogate, it even fails to find a solution satisfying the design specifications. The trust-region-enhanced algorithms perform well ensuring both algorithm convergence and a high-quality final design. The fine model responses: the initial and optimal designs obtained using the $\mathrm{SM_{TR-B2}}$ algorithm with the $\boldsymbol{R}_{c.I}(\boldsymbol{x})$ model are shown in Fig. 10. Convergence plots for $\mathrm{SM_{STD}}$ and $\mathrm{SM_{TR-B2}}$ working with the implicit space-mapping surrogate $\boldsymbol{R}_{c.I}(\boldsymbol{x})$ are shown in Fig. 11.

D. Open-Loop Ring Resonator Bandpass Filter [36]

Our final example is the open-loop ring resonator bandpass filter [36] (Fig. 12). The design parameters are $\boldsymbol{x} = [L_1\ L_2\ L_3\ L_4\ S_1\ S_2\ g]^T$ mm. Other parameter values are $W = 0.6$ mm, $W_1 = 0.4$ mm. $\boldsymbol{R}_f$ is simulated in FEKO [34]. The coarse model (Fig. 13) is implemented in Agilent ADS [32]. The design specifications are $|S_{21}| \geq -3$ dB for 2.8 GHz $\leq \omega \leq$ 3.2 GHz, and $|S_{21}| \leq -20$ dB for

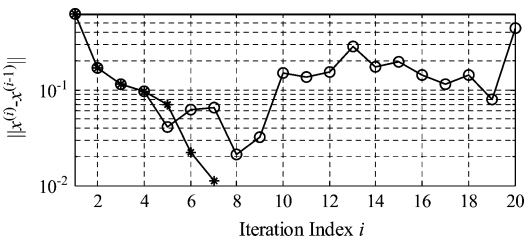

Fig. 11. Wideband ring resonator filter: convergence plots for $\mathrm{SM_{STD}}(\mathrm{o})$ and $\mathrm{SM_{TR-B2}}(*)$, both using surrogate model $\boldsymbol{R}_{c.I}(\boldsymbol{x})$, versus iteration index.

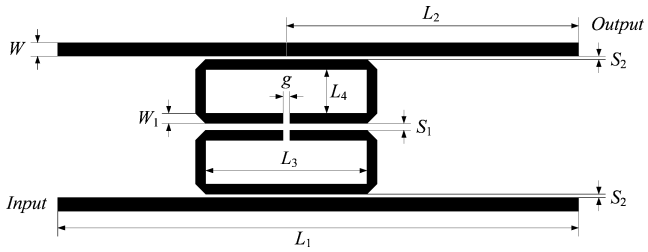

Fig. 12. Open-loop ring resonator bandpass filter: geometry [36].

1.5 GHz $\leq \omega \leq$ 2.5 GHz and 3.5 GHz $\leq \omega \leq$ 4.5 GHz. The initial design is the coarse model optimal solution $\boldsymbol{x}^{(0)} = [39.389\ 8.987\ 5.036\ 4.553\ 0.268\ 0.100\ 1.000]^T$ mm (specification error + 11.8 dB).

Here, we use the following surrogate models: the frequency space-mapping model $\bar{\boldsymbol{R}}_s(\boldsymbol{x}) = \boldsymbol{R}_{c.F}(\boldsymbol{x})$, and the implicit space-mapping model $\bar{\boldsymbol{R}}_s(\boldsymbol{x}) = \boldsymbol{R}_{c.I}(\boldsymbol{x})$ with the substrate height and dielectric constants used as preassigned parameters [22].

The optimization results are shown in Table IV. For this problem, the standard space-mapping algorithm does not perform well when the frequency space-mapping surrogate is used; however, it is as good as the trust-region-enhanced algorithms for the implicit space-mapping surrogate. This indicates that, in a way, the trust-region mechanism is being "turned on" only if necessary; otherwise, it does not interfere with the space-mapping optimization process. Fig. 14 shows the initial and final fine model responses for the $\mathrm{SM_{TR-B2}}$ algorithm with the $\boldsymbol{R}_{c.I}(\boldsymbol{x})$ model. Fig. 15 shows the evolution of the specification error for $\mathrm{SM_{STD}}$ and $\mathrm{SM_{TR-B2}}$ algorithm using the $\boldsymbol{R}_{c.F}(\boldsymbol{x})$ model. This figure illustrates a quite common behavior of the standard space-mapping algorithm: after initial success, the algorithm may not be able to yield further improvement if the surrogate model type is not properly selected.

E. Discussion

The numerical results presented in Sections IV-A–IV-D indicate the advantages of the trust-region-enhanced space-mapping algorithms $\mathrm{SM_{TR}}$, $\mathrm{SM_{TR-B1}}$ and $\mathrm{SM_{TR-B2}}$ over the standard space-mapping algorithm $\mathrm{SM_{STD}}$. The results can be summarized as follows.

(a) Algorithms $\mathrm{SM_{TR}}$, $\mathrm{SM_{TR-B1}}$, and $\mathrm{SM_{TR-B2}}$ ensure convergence for all considered test problems, which is not the case for the standard space-mapping algorithm.

(b) In many cases, the basic trust-region algorithm $\mathrm{SM_{TR}}$ performs as well as the algorithms using the Jacobian estimation ($\mathrm{SM_{TR-B1}}$ and $\mathrm{SM_{TR-B2}}$), however, in some cases, the latter approach prevails: the $\mathrm{SM_{TR}}$ algorithm may simply get stuck because the property $U(\boldsymbol{R}_f(\boldsymbol{x}^{(i+1)})) < U(\boldsymbol{R}_f(\boldsymbol{x}^{(i)}))$ may not hold even for very small trust-region radius values (cf. Section III-C).

(c) Algorithms $\mathrm{SM_{TR-B1}}$ and $\mathrm{SM_{TR-B2}}$ can be considered as equally good; the small differences in the final design

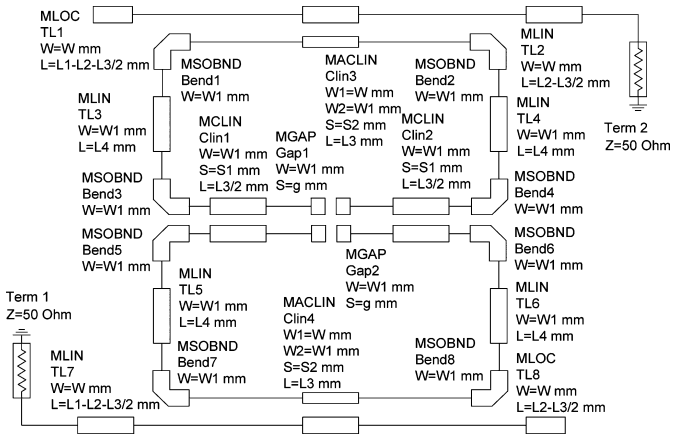

Fig. 13. Open-loop ring resonator bandpass filter: coarse model (Agilent ADS).

TABLE IV
OPEN-LOOP RING RESONATOR FILTER: OPTIMIZATION RESULTS[22]

Surrogate Model	SM Algorithm	Specification Error		Number of Fine Model Evaluations
		Final	Best Found	
$\boldsymbol{R}_{c.F}(\boldsymbol{x})$	$\mathrm{SM_{STD}}$	+0.6	−0.9	21[#]
	$\mathrm{SM_{TR}}$	−1.2	−1.2	11
	$\mathrm{SM_{TR\text{-}B1}}$	−1.2	−1.2	11
	$\mathrm{SM_{TR\text{-}B2}}$	−1.2	−1.2	11
$\boldsymbol{R}_{c.I}(\boldsymbol{x})$	$\mathrm{SM_{STD}}$	−1.8	−1.8	12
	$\mathrm{SM_{TR}}$	−1.8	−1.8	6
	$\mathrm{SM_{TR\text{-}B1}}$	−1.8	−1.8	6
	$\mathrm{SM_{TR\text{-}B2}}$	−1.8	−1.8	8

[#] Convergence not obtained; algorithm terminated after 20 iterations.

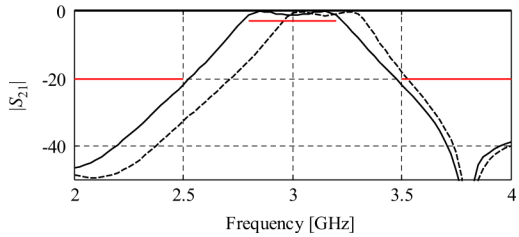

Fig. 14. Open-loop ring resonator filter: initial (dashed line) and optimized (solid line) $|S_{21}|$ versus frequency; optimization using the $\mathrm{SM_{TR-B2}}$ algorithm with the $\boldsymbol{R}_{c.I}(\boldsymbol{x})$ model [22].

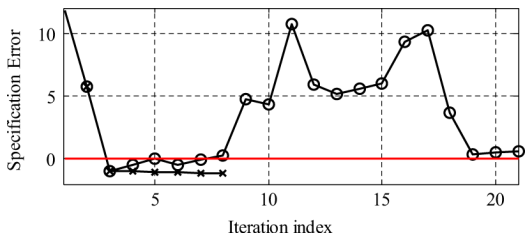

Fig. 15. Open-loop ring resonator filter: evolution of the specification error for $\mathrm{SM_{STD}}(\mathrm{o})$ and $\mathrm{SM_{TR-B2}}(\times)$, both using surrogate model $\boldsymbol{R}_{c.F}(\boldsymbol{x})$ versus iteration index [22].

quality and the computational cost of the optimization process come from different ways of implementing the $\boldsymbol{E}$-term in model (10) (cf. Section III).

(d) In the cases when the $\mathrm{SM_{STD}}$ does well, both $\mathrm{SM_{TR}}$ and $\mathrm{SM_{TR-B1}}/\mathrm{SM_{TR-B2}}$ have little or no effect, which is exactly what we require.

(e) Using trust-region-enhancement makes the space-mapping algorithm less sensitive to the selection of surrogate model type: $\mathrm{SM_{STD}}$ may perform well for certain surrogate model types and poorly for others, see Tables I–IV; performance differences are much less pronounced in trust-region enhanced algorithms.

These conclusions are in agreement with theoretical predictions. In particular, the convergence of the trust-region-enhanced algorithms, as well as iteration-to-iteration improvement with respect to the specification error value (cf. Fig. 15) is ensured by the trust-region mechanism itself. On the other hand, extra information in the form of the fine/surrogate model Jacobian estimation allows further improvement of the final design quality because the fundamental property $U(\boldsymbol{R}_f(\boldsymbol{x}^{(i+1)})) < U(\boldsymbol{R}_f(\boldsymbol{x}^{(i)}))$ is ensured for sufficiently small trust-region radius.

V. Conclusion

A systematic treatment of trust-region-enhanced space-mapping algorithms is presented. A basic trust-region space-mapping algorithm and its extensions exploiting the fine model Jacobian estimation are considered. An extensive performance comparison with the standard algorithm indicates that the trust region approach discussed in this paper can be considered as an important step toward improving the robustness of the space-mapping optimization process.

Appendix

We provide an analytical argument showing that the modified trust-region-enhanced space-mapping algorithms of Sections III-A and III-B ensure improvement of the fine model objective function, i.e., $U(\boldsymbol{R}_f(\boldsymbol{x}^{(i+1)})) < U(\boldsymbol{R}_f(\boldsymbol{x}^{(i)}))$, provided that the trust-region radius $\delta^{(i)}$ [cf. (5)] is sufficiently small.

We assume, for simplicity, that the merit function U is smooth. Suppose that the optimization of the surrogate model $\boldsymbol{R}_s^{(i)}$ produces a new iteration point $\boldsymbol{x}^{(i+1)}$ such that $U(\boldsymbol{R}_f(\boldsymbol{x}^{(i+1)})) > U(\boldsymbol{R}_f(\boldsymbol{x}^{(i)}))$. Design $\boldsymbol{x}^{(i+1)}$ must be then rejected and model $\boldsymbol{R}_s^{(i)}$ will be updated [e.g., using (10), (11), (15) or (10), (11), (17)] so that the following relation holds $\boldsymbol{R}_f(\boldsymbol{x}^{(i+1)}) - \boldsymbol{R}_f(\boldsymbol{x}^{(i)}) \approx \boldsymbol{J}_{\boldsymbol{R}_s^{(i)}}(\boldsymbol{x}^{(i)}) \cdot (\boldsymbol{x}^{(i+1)} - \boldsymbol{x}^{(i)})$ for a sufficiently small $\delta^{(i)}$. In particular, we have that $\boldsymbol{J}_{\boldsymbol{R}_s^{(i)}}(\boldsymbol{x}^{(i)})\big|_{\boldsymbol{h}^{(i)}} \approx \boldsymbol{J}_{\boldsymbol{R}_f}(\boldsymbol{x}^{(i)})\big|_{\boldsymbol{h}^{(i)}}$, where $\boldsymbol{J}_{(\cdot)}\big|_{\boldsymbol{h}^{(i)}}$ denotes the directional derivative along $\boldsymbol{h}^{(i)} = \boldsymbol{x}^{(i+1)} - \boldsymbol{x}^{(i)}$. Now, again for the trust-region radius $\delta^{(i)}$ being sufficiently small, the optimal solution $\bar{\boldsymbol{x}}^{(i+1)}$ of the updated surrogate will be located almost on the line defined as $\boldsymbol{x}^{(i)} + t(\boldsymbol{x}^{(i+1)} - \boldsymbol{x}^{(i)})$, $t \in R$. More specifically, $\bar{\boldsymbol{x}}^{(i+1)} \approx \boldsymbol{x}^{(i)} + c \cdot (\boldsymbol{x}^{(i)} - \boldsymbol{x}^{(i+1)})$ with $c = \delta^{(i)}/\|\boldsymbol{x}^{(i+1)} - \boldsymbol{x}^{(i)}\| > 0$. We have the following relation (∇U denotes the gradient of U at $\boldsymbol{x}^{(i)}$): $U(\boldsymbol{R}_f(\bar{\boldsymbol{x}}^{(i+1)})) \approx U(\boldsymbol{R}_f(\boldsymbol{x}^{(i)})) + \nabla U\, \boldsymbol{J}_{\boldsymbol{R}_f}(\boldsymbol{x}^{(i)})\big|_{\boldsymbol{h}^{(i)}} \cdot (\bar{\boldsymbol{x}}^{(i+1)} - \boldsymbol{x}^{(i)}) \approx U(\boldsymbol{R}_f(\boldsymbol{x}^{(i)})) - c \cdot \nabla U\, \boldsymbol{J}_{\boldsymbol{R}_s^{(i)}}(\boldsymbol{x}^{(i)})\big|_{\boldsymbol{h}^{(i)}} \cdot (\boldsymbol{x}^{(i+1)} - \boldsymbol{x}^{(i)})$, which gives $U(\boldsymbol{R}_f(\bar{\boldsymbol{x}}^{(i+1)})) \approx U(\boldsymbol{R}_f(\boldsymbol{x}^{(i)})) - c \cdot \nabla U(\boldsymbol{R}_f(\boldsymbol{x}^{(i+1)}) - \boldsymbol{R}_f^{(i)}(\boldsymbol{x}^{(i)}))$, and finally, $U(\boldsymbol{R}_f(\bar{\boldsymbol{x}}^{(i+1)})) \approx U(\boldsymbol{R}_f(\boldsymbol{x}^{(i)})) - c \cdot (U(\boldsymbol{R}_f(\boldsymbol{x}^{(i+1)})) - U(\boldsymbol{R}_f^{(i)}(\boldsymbol{x}^{(i)}))) < U(\boldsymbol{R}_f(\boldsymbol{x}^{(i)}))$, as we assumed $U(\boldsymbol{R}_f(\boldsymbol{x}^{(i+1)})) > U(\boldsymbol{R}_f(\boldsymbol{x}^{(i)}))$.

Acknowledgment

The authors thank Sonnet Software Inc., Syracuse, NY, for making ***em*** available, and Agilent Technologies, Santa Rosa, CA, for making ADS available.

References

[1] S. Koziel, Q. S. Cheng, and J. W. Bandler, "Space mapping," *IEEE Microw. Mag.*, vol. 9, no. 6, pp. 105–122, Dec. 2008.

[2] J. W. Bandler, Q. S. Cheng, S. A. Dakroury, A. S. Mohamed, M. H. Bakr, K. Madsen, and J. Sondergaard, "Space mapping: The state of the art," *IEEE Trans. Microw. Theory Tech.*, vol. 52, no. 1, pp. 337–361, Jan. 2004.

[3] S. Koziel, J. W. Bandler, and K. Madsen, "A space mapping framework for engineering optimization: Theory and implementation," *IEEE Trans. Microw. Theory Tech.*, vol. 54, no. 10, pp. 3721–3730, Oct. 2006.

[4] D. Echeverria and P. W. Hemker, "Space mapping and defect correction," *Int. Math. J. Comput. Methods Appl. Math.*, vol. 5, no. 2, pp. 107–136, 2005.

[5] M. A. Ismail, D. Smith, A. Panariello, Y. Wang, and M. Yu, "EM-based design of large-scale dielectric-resonator filters and multiplexers by space mapping," *IEEE Trans. Microw. Theory Tech.*, vol. 52, no. 1, pp. 386–392, Jan. 2004.

[6] K.-L. Wu, Y.-J. Zhao, J. Wang, and M. K. K. Cheng, "An effective dynamic coarse model for optimization design of LTCC RF circuits with aggressive space mapping," *IEEE Trans. Microw. Theory Tech.*, vol. 52, no. 1, pp. 393–402, Jan. 2004.

[7] J. E. Rayas-Sánchez, F. Lara-Rojo, and E. Martínez-Guerrero, "A linear inverse space mapping (LISM) algorithm to design linear and nonlinear RF and microwave circuits," *IEEE Trans. Microw. Theory Tech.*, vol. 53, no. 3, pp. 960–968, Mar. 2005.

[8] M. Dorica and D. D. Giannacopoulos, "Response surface space mapping for electromagnetic optimization," *IEEE Trans. Magn.*, vol. 42, no. 4, pp. 1123–1126, Apr. 2006.

[9] S. Amari, C. LeDrew, and W. Menzel, "Space-mapping optimization of planar coupled-resonator microwave filters," *IEEE Trans. Microw. Theory Tech.*, vol. 54, no. 5, pp. 2153–2159, May 2006.

[10] D. Echeverria, D. Lahaye, L. Encica, E. A. Lomonova, P. W. Hemker, and A. J. A. Vandenput, "Manifold-mapping optimization applied to linear actuator design," *IEEE Trans. Magn.*, vol. 42, no. 4, pp. 1183–1186, Apr. 2006.

[11] G. Crevecoeur, P. Sergeant, L. Dupre, and R. Van de Walle, "Two-level response and parameter mapping optimization for magnetic shielding," *IEEE Trans. Magn.*, vol. 44, no. 2, pp. 301–308, Feb. 2008.

[12] M. F. Pantoja, P. Meincke, and A. R. Bretones, "A hybrid genetic-algorithm space-mapping tool for the optimization of antennas," *IEEE Trans. Antennas Propag.*, vol. 55, no. 3, pp. 777–781, Mar. 2007.

[13] P. Sergeant, R. V. Sabariego, G. Crevecoeur, L. Dupre, and C. Geuzaine, "Analysis of perforated magnetic shields for electric power applications," *IET Elect. Power Appl.*, vol. 3, no. 2, pp. 123–132, Mar. 2009.

[14] V. K. Devabhaktuni, B. Chattaraj, M. C. E. Yagoub, and Q.-J. Zhang, "Advanced microwave modeling framework exploiting automatic model generation, knowledge neural networks, and space mapping," *IEEE Trans. Microw. Theory Tech.*, vol. 51, no. 7, pp. 1822–1833, Jul. 2003.

[15] J. C. Rautio, "A space mapped model of thick, tightly coupled conductors for planar electromagnetic analysis," *IEEE Microw. Mag.*, vol. 5, no. 3, pp. 62–72, Sep. 2004.

[16] L. Zhang, J. Xu, M. C. E. Yagoub, R. Ding, and Q.-J. Zhang, "Efficient analytical formulation and sensitivity analysis of neuro-space mapping for nonlinear microwave device modeling," *IEEE Trans. Microw. Theory Tech.*, vol. 53, no. 9, pp. 2752–2767, Sep. 2005.

[17] N. M. Alexandrov and R. M. Lewis, "An overview of first-order model management for engineering optimization," *Optim. Eng.*, vol. 2, no. 4, pp. 413–430, Dec. 2001.

[18] A. J. Booker, J. E. Dennis, Jr., P. D. Frank, D. B. Serafini, V. Torczon, and M. W. Trosset, "A rigorous framework for optimization of expensive functions by surrogates," *Struct. Optim.*, vol. 17, no. 1, pp. 1–13, Feb. 1999.
[19] J. E. Dennis and V. Torczon, "Managing approximation models in optimization," in *Multidisciplinary Design Optimization*, N. M. Alexrov and M. Y. Hussaini, Eds. Philadelphia, PA: SIAM, 1997, pp. 330–374.
[20] N. V. Queipo, R. T. Haftka, W. Shyy, T. Goel, R. Vaidynathan, and P. K. Tucker, "Surrogate-based analysis and optimization," *Progr. Aerosp. Sci.*, vol. 41, no. 1, pp. 1–28, Jan. 2005.
[21] S. Koziel, J. W. Bandler, and K. Madsen, "Quality assessment of coarse models and surrogates for space mapping optimization," *Optim. Eng.*, vol. 9, no. 4, pp. 375–391, 2008.
[22] S. Koziel, J. W. Bandler, and Q. S. Cheng, "Trust-region-based convergence safeguards for space mapping design optimization of microwave circuits," in *IEEE MTT-S Int. Microw. Symp. Dig*, Boston, MA, 2009, pp. 1261–1264.
[23] S. Koziel and J. W. Bandler, "Space-mapping optimization with adaptive surrogate model," *IEEE Trans. Microw. Theory Tech.*, vol. 55, no. 3, pp. 541–547, Mar. 2007.
[24] A. R. Conn, N. I. M. Gould, and P. L. Toint, *Trust Region Methods*, ser. MPS-SIAM Optimization. Philadelphia, PA: , 2000.
[25] M. H. Bakr, J. W. Bandler, R. M. Biernacki, S. H. Chen, and K. Madsen, "A trust region aggressive space mapping algorithm for EM optimization," *IEEE Trans. Microw. Theory Tech.*, vol. 46, no. 12, pp. 2412–2425, Dec. 1998.
[26] N. M. Alexandrov, J. E. Dennis, R. M. Lewis, and V. Torczon, "A trust region framework for managing use of approximation models in optimization," *Struct. Multidisciplinary Optim.*, vol. 15, no. 1, pp. 16–23, 1998.
[27] J. W. Bandler, Q. S. Cheng, N. K. Nikolova, and M. A. Ismail, "Implicit space mapping optimization exploiting preassigned parameters," *IEEE Trans. Microw. Theory Tech.*, vol. 52, no. 1, pp. 378–385, Jan. 2004.
[28] N. K. Nikolova, Y. Li, Y. Li, and M. H. Bakr, "Sensitivity analysis of scattering parameters with electromagnetic time-domain simulators," *IEEE Trans. Microw. Theory Tech.*, vol. 54, no. 4, pp. 1598–1610, Apr. 2006.
[29] C. G. Broyden, "A class of methods for solving nonlinear simultaneous equations," *Math. Comput.*, vol. 19, pp. 577–593, 1965.
[30] J. T. Kuo, S. P. Chen, and M. Jiang, "Parallel-coupled microstrip filters with over-coupled end stages for suppression of spurious responses," *IEEE Microw. Wireless Compon. Lett.*, vol. 13, no. 10, pp. 440–442, Oct. 2003.
[31] ***em***. ver. 11.54, Sonnet Softw. Inc., North Syracuse, NY, 2008.
[32] Agilent ADS. ver. 2008, Agilent Technol., Santa Rosa, CA, 2008.
[33] M. H. M. Salleh, G. Prigent, O. Pigaglio, and R. Crampagne, "Quarter-wavelength side-coupled ring resonator for bandpass filters," *IEEE Trans. Microw. Theory Tech.*, vol. 56, no. 1, pp. 156–162, Jan. 2008.
[34] *"FEKO® User's Manual,"* EM Software & Syst. S.A. (Pty) Ltd., Stellenbosch, South Africa, 2008.
[35] S. Sun and L. Zhu, "Wideband microstrip ring resonator bandpass filters under multiple resonances," *IEEE Trans. Microw. Theory Tech.*, vol. 55, no. 10, pp. 2176–2182, Oct. 2007.
[36] C. Y. Chen and C. Y. Hsu, "A simple and effective method for microstrip dual-band filters design," *IEEE Microw. Wireless Compon. Lett.*, vol. 16, no. 5, pp. 246–248, May 2006.

Slawomir Koziel (M'03–SM'07) received the M.Sc. and Ph.D. degrees in electronic engineering from Gdansk University of Technology, Gdansk, Poland, in 1995 and 2000, respectively, and the M.Sc. degrees in theoretical physics and in mathematics and Ph.D. degree in mathematics from the University of Gdansk, Gdansk, Poland, in 2000, 2002, and 2003, respectively.

He is currently an Associate Professor with the School of Science and Engineering, Reykjavik University, Reykjavik, Iceland. His research interests include computer-aided design (CAD) and modeling of microwave circuits, surrogate-based optimization, space mapping, circuit theory, analog signal processing, evolutionary computation, and numerical analysis.

John W. Bandler (S'66–M'66–SM'74–F'78–LF'06) studied at Imperial College, London, U.K. He received the B.Sc. (Eng.), Ph.D., and D.Sc.(Eng.) degrees from the University of London, London, U.K., in 1963, 1967, and 1976, respectively.

In 1969, he joined McMaster University, Hamilton, ON, Canada, where he is currently a Professor Emeritus. He was President of Optimization Systems Associates Inc., which he founded in 1983, until November 20, 1997 (the date of acquisition by the Hewlett-Packard Company). He is President of Bandler Corporation, Dundas, ON, Canada, which he founded in 1997.

Dr. Bandler is a Fellow of several societies including the Royal Society of Canada. He was the recipient of the 2004 IEEE Microwave Theory and Techniques Society (IEEE MTT-S) Microwave Application Award.

Qingsha S. Cheng (S'00–M'05–SM'09) was born in Chongqing, China. He received the B.Eng. and M.Eng. degrees from Chongqing University, Chongqing, China, in 1995 and 1998, respectively, and the Ph.D. degree from McMaster University, Hamilton, ON, Canada, in 2004.

In 1998, he joined the Department of Computer Science and Technology, Peking University, Beijing, China. In 1999, he joined the Department of Electrical and Computer Engineering, McMaster University, where he is currently a Research Associate with the Department of Electrical and Computer Engineering and a Lecturer with the Faculty of Engineering. His research interests are surrogate modeling, computer-aided design (CAD), modeling of microwave circuits, software design technology, and methodologies for microwave CAD.